Polyhedra Formation and Transient Cone Ejection of a Resonant Microdrop Forced by an ac Electric Field

Ping Wang, Siddharth Maheshwari, and Hsueh-Chia Chang

Center for Microfluidics and Medical Diagnostics, Department of Chemical and Biomolecular Engineering, University of Notre Dame, Notre Dame, Indiana 46556, USA

(Received 14 February 2006; revised manuscript received 9 May 2006; published 27 June 2006)

New deformation or fission phenomena are reported for microdrops driven by an ac electric field at their resonant frequencies. The Maxwell forces that pull out the vertices from a drop can be enhanced when the ac frequency is comparable to both the drop resonant frequency and the inverse charge relaxation time of the diffuse layer. The selected polyhedra possess symmetries that ensure a global force balance of the Maxwell forces and a linear dimension consistent with a sphere whose nth harmonic (n is up to six in the observation) coincides with the applied ac frequency. At high voltages, the resonant focusing of charges by the vibration modes produces evenly distributed and transient Taylor cones that can eject charged nanodrops.

DOI: 10.1103/PhysRevLett.96.254502 PACS numbers: 47.61.Fg, 47.20.Ma, 77.22.Ej

The use of dc electric fields to atomize liquid drops from Taylor cones is widely used in protein and DNA characterization [1], microencapsulation [2], nanotechnology [3], etc., due to its ability to produce nanosized mono- and polydispersed drops. Such electrospraying phenomena employ the concentrated electric field and polarization at the Taylor cone to eject micron-sized drops. The ejected charged drops undergo Rayleigh fission and can eventually reach nanometer size. With the exception of a few recent studies [4], earlier works on electrosprays have focused on dc sprays [5] or ac sprays at frequencies (>10 kHz) much higher than the drop resonant frequency [6]. In this Letter, we examine the consequence when the drop resonance is used to focus the polarization and Maxwell forces on a microdrop by employing a designated ac frequency. At discrete drop sizes and frequencies, specific spherical harmonics are shown to evolve into specific polyhedra at comparatively low voltages and develop into multiple transient Taylor cones at higher voltages. The onset voltages for transient cones are also found to be lower than their dc counterpart due to the resonance enhanced effects.

Traditional dc sprays are known to produce a well-defined Taylor cone with a half angle close to the Taylor angle of 49.3° for highly conductive liquids [7]. After charge relaxation, a diffuse-layer–type polarization is generated due to the liquid electric field, and the charge can be focused by interfacial singularities like sharp cones and wedges, the Taylor cone being one example. In contrast, high-frequency ac sprays, with the applied frequency higher than a critical value, and their driving Maxwell force have been attributed to gas-phase polarization due to gas volume ionization reactions [8]. In addition, high-frequency ac sprays generally do not involve well-defined Taylor cones, which are characteristic of the predominant stable cone jet in dc spray. However, at low frequencies, liquid phase charge separation and accumulation behavior, analogous to dc-type behavior, is possible and nontrivial drop shapes and dynamic electrosprays can be excited. But besides charge separation, resonant vibration can also be induced at specific low frequency ac fields, since the natural vibration frequency of the drop and its overtones can coincide with the applied frequency. In addition, ac-induced Maxwell force on an electrode exhibits a maximum at a frequency near the inverse charging time due to a diffuse layer screening effect [9]. Hence, by using microdrops and low ac frequency such that the latter matches the drop resonant frequency and the diffuse layer charging time, we observe resonating polyhedral drops which give rise to multiple transient Taylor cones on the interface with increase in voltage. We shall begin by describing the experimental setup and results followed by an attempt to explain the observed phenomena with scaling laws.

Our experimental setup resembles the conventional dc spray experiments. A sinusoidal ac signal was generated by a function/arbitrary waveform generator (Agilent 33220 A) and magnified through a rf amplifier (Powertron 250 A) and a secondary high voltage transformer (Industrial Test Equipment, 0.1–10 kHz), capable of delivering up to $10\,000 V_{\text{peak-peak}}$. A steel microneedle (Hamilton, 91033) with nominal outer diameter 210 μm and thickness 50 μm was filled with the working fluid and mounted obliquely with an angle of 45° to the horizontal plane such that a nanoliter-sized drop could be extracted from it. The needle inclination is variable and was introduced to supply liquid by drainage during the ejection events, but the inclination angle is found to have little effect on the observed phenomena. The counterelectrode consisted of a strip of copper tape placed 10 mm away from the needle tip. The applied voltage and frequency were monitored by a high voltage ac probe (Tektronix, P6015A) linked with an oscilloscope. The entire phenomenon was imaged by an inverted microscope (Olympus IX-71) and recorded using a high-speed camera (Olympus i speed) at 500–6000 frames/s. The working liquid is acetonitrile (Sigma, 99.5% +), with surface tension $\sigma \sim 19$ mN/m, density $\rho \sim 783$ kg/m^3, viscosity $\mu \sim 0.38$ mPa s, and

relative permittivity $\varepsilon_r \sim 37$. The reason for utilizing pure fluids of low surface tension instead of surfactant solutions is to exclude surface tension gradients due to nonuniform distribution of surfactant molecules under a focused electric field.

For microdrops with dimensions smaller than the capillary length $R_c = (\sigma/\rho g)^{1/2}$, approximately 1.5 mm for acetonitrile, gravitational effects are negligible and the resulting spherical drops with a radius R possess discrete resonant frequencies. The resonant modes exhibit the following resonant frequencies given by the Rayleigh-Lamb (RL) dispersion relationship for the inviscid case,

$$f_n = \frac{1}{2\pi}\sqrt{\frac{n(n-1)(n+2)\sigma}{\rho R^3}}, \qquad (1)$$

where the integer n ($n \neq 1$) indicates the polar wave number. We also note that this is independent of the azimuthal wave number, m [10]. The fundamental frequency at $n = 1$ is $2\pi f_1 = (\sigma/\rho R^3)^{1/2}$, corresponding to an isolated sphere. The fundamental frequency f_1 is plotted vs R in Fig. 1(a) for acetonitrile that allows us to design the appropriate resonant experiments. The low viscosity value of acetonitrile also makes the comparison with the present inviscid results meaningful. The capillary wave speed, v_0, given by $v_0 = (2\sigma/\rho R)^{1/2}$ was found to be about 48 cm/s, where R is taken as 200 μm. The Reynolds number $\rho v_0 R/\mu$ was then calculated to be $\sim$260, which is also consistent with the inviscid approximation made in this work.

There are, however, constraints that impose specific windows on the drop size and the correlated ac frequency f through (1). The upper bound on R is for a sphere with a radius equal to the capillary length R_c; the corresponding resonant frequency f_c is about 150 Hz. Above this radius, gravity dominates and severe liquid dripping occurs to prevent the formation of a spherical drop. The lower bound on R is imposed by an upper bound on f via an induced-charge polarization mechanism [11]. As there is a finite charge accumulation time for the diffuse layer polarization at the liquid-air interface, the applied frequency has this upper cutoff. From the liquid conductivity, an ionic concentration, c, of roughly 10^{-7} M is obtained, from which we deduce the diffuse layer thickness, $\lambda = [(\varepsilon_l R_g T)/(2F^2 z^2 c)]^{1/2}$, to be approximately 0.4 μm, ε_l being the liquid permittivity, R_g the molar gas constant, T the absolute temperature, F the Faraday constant, and z the ionic valency. An "RC time," which arises from the coupling between diffuse layer "capacitor" charging and the bulk "resistor" supplying the electric field and current, can be estimated to be $T_{DL} \sim \lambda R/D$, or 10^{-3} s, D being the ionic diffusivity. If f is much larger than the corresponding charging frequency of $f_{DL} \sim 1/T_{DL} = 1$ kHz, the interface is not fully polarized at each half cycle to produce the driving Maxwell force. Figure 1(b) depicts the measured phase angle and admittance of the spray system as a function of frequency. As f increase from 0.1 to 10 kHz, the phase angle drops from 90° to almost 0°, corresponding to the transition from a resistor dominant system to a capacitor dominant system. This result is consistent with the estimated RC time scale.

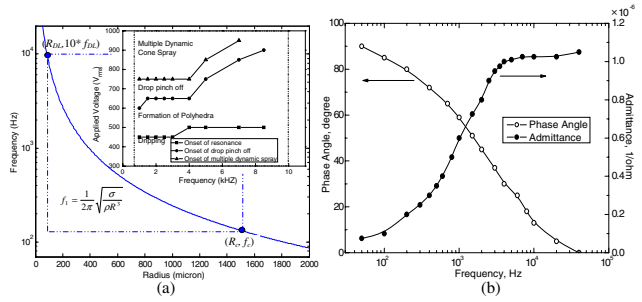

FIG. 1 (color online). (a) The operating frequency and drop windows for resonant vibration. The segment of the line between $(R_{\mathrm{DL}}, 10^* f_{\mathrm{DL}})$ and (R_c, f_c) denotes the resonant regime. The inset shows the applied voltage windows for the several drop behaviors as a function of frequency. The drop exhibits dripping, polyhedral deformation, drop pinch off, and multiple transient sprays successively as the applied voltage is increased. (b) The measured phase angle and admittance of the spray system as a function of applied frequency.

There is also a specific voltage window for the observation of polyhedral drops. As has been seen with mechanical excitation, at the resonant frequency the drops are deformed and vibrate with the applied frequency. However, in addition, the applied electric field induces liquid phase charge separation, similar to that observed in dc electrospraying, and the charges can get focused on the antinodes of the polyhedral shape, akin to charge focusing in the Taylor cone. At comparatively lower voltages, capillary forces are dominant and can manage to prevent drop break up, and polyhedral drop shapes can be retained. At higher voltages, polarization can no longer be balanced by capillary forces, and drop break up and ejection takes place, as seen in the inset of Fig. 1(a). We also note the weak increase in voltage for the polyhedra regime with frequency. This trend reflects the fact that the Maxwell forces that deform the drop into polyhedra and the vertices into jets must overcome interfacial capillary forces. As the drop size R decreases with f according to the RL dispersion relationship, the restraining capillary force increases and larger voltages are necessitated.

Figure 2(a) depicts the successively evolved polyhedral drops (polygonal shape in two-dimension projection) observed at a frequency of 1 kHz and their corresponding polar mode number n. The drops were first pulled out of the capillary by a net longitudinal Maxwell force supplied by the ac field of frequency f in each experiment. They then undergo discrete resonant vibration when their growing radius R satisfies Eq. (1) for a given integer n. The inclination angle of the needle was also set to 0° and nearly 90° relative to the horizontal plane yielding no significant difference in the results, confirming that three-dimensional

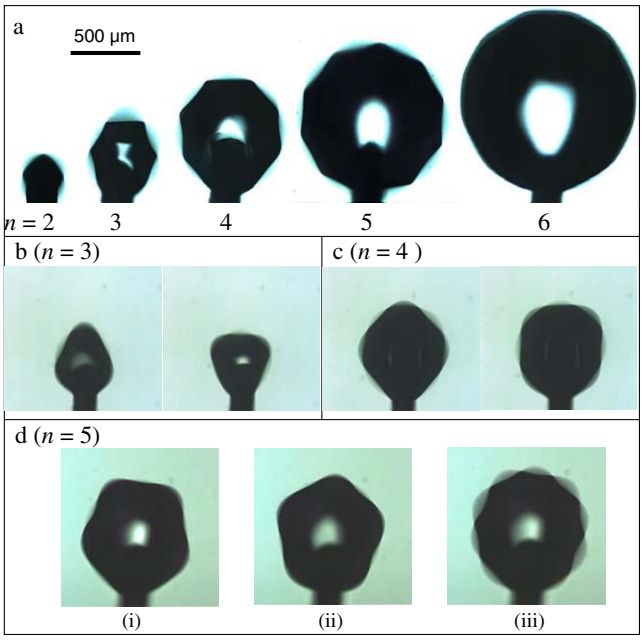

FIG. 2 (color online). Resonant deformation of an acetonitrile drop into polyhedra at a needle orifice. Experimental parameters: electric field, $E_\infty \approx 0.7$ kV/cm, forcing frequency $f = 1$ kHz. Similar polyhedra are observed for several discrete frequencies between 0.5 to 7 kHz. (a) Close-up images of a single drop at different resonant modes induced by the applied electric field. From the left to right are $n = 2$, 3, 4, 5, and 6, respectively. (b)–(d) High-speed images illustrating the standing wave pattern with $n = 3$, 4 and 5, respectively. The image of (iii) in (d) is a composite of (i) and (ii).

polyhedral shapes are obtained. The voltage was adjusted such that drop growth was slow enough to allow resonant modes to appear at specific drop volumes and fast enough to neutralize liquid evaporation. The expanding drop exhibited abrupt transitions from its spherical shape into polyhedra that lasted around 10–100 ms during its path through the various discrete resonance events. In between each resonance event, the drop spontaneously relaxed back to the spherical shape due to capillarity. Unlike other vibration methods induced by acoustic or piezoelectric or ultrasonic wave [12,13], remarkable protuberances were generated on the interface during resonance. Similar passage through resonance was obtained at frequencies between 500 Hz and 7 kHz, with different drop dimensions.

Careful observation reveals that these meniscus "protuberances" in Fig. 2(a) are actually nodes of resonant standing waves. Since these images were obtained at a frame rate of 1000 frames/s, which is exactly the same as the applied frequency, and since polyhedral structures are obtained every half cycle, the presented images are actually overlaps of 2 successive polyhedral images. In fact, the high-speed images shown in Figs. 2(b)–2(d) demonstrate two standing wave patterns formed at each half cycle with mode numbers $n = 3$, 4 and 5, respectively. Overlapping of first two images (i) and (ii) in (d) gives rise to the image of (iii) that resembles the higher order polyhedra shown in (a).

At low amplitudes, the drop oscillation can be described in terms of the spherical harmonics and Legendre polynomials $\Delta R \sim P_n^m(\theta)e^{\pm im\varphi}$, where P_n^m is Legendre polynomial, φ is the azimuthal angle, and θ is the polar angle. For each n there exists one axisymmetric oscillation mode and $2n$ distinct three-dimensional modes. However, only specific polyhedra, corresponding to particular modes, are observed out of this multiplicity of modes. This effect is not fully understood. A possible explanation is the following: within each half cycle, the charges are distributed at the various antinodes of the meniscus forming singular Maxwell forces at the sharp vertices. For stable polyhedra, these point forces should sum up to zero and this equilibrium of vertex point forces can be achieved only with the observed shapes, which are highly symmetrical. Nevertheless, a deeper investigation is required to clarify this behavior.

Figure 3(a) shows both the measured and the theoretical drop radius calculated from RL dispersion relation at a frequency of 1 kHz as a function of the wave mode number. In fact, the theoretical trend line is very close to a straight line for small mode numbers. Our measurements agree with theoretical values quantitatively in the middle range, while the deviation increases for larger and small mode number at the two ends. Since the RL dispersion relationship is for a free drop, while in our experiments the drops are suspended from a needle, we have also compared the observed drop dimension with the drop dimension predicted by the "constrained drop model" [14]. At low

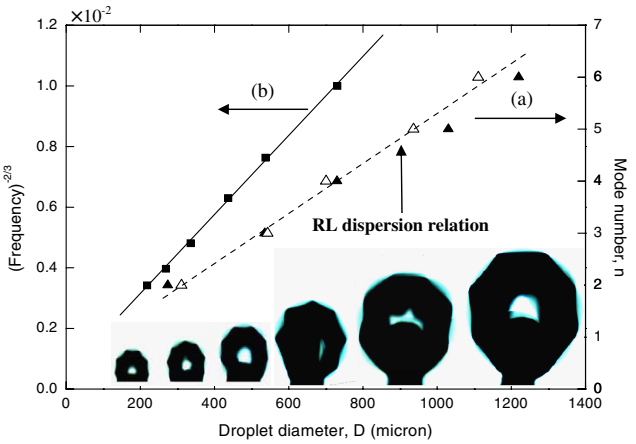

FIG. 3 (color online). (a) Observed resonant drop diameter (▲) and calculated resonant drop diameter (△) from a constrained drop model as a function of the mode number n. The frequency is fixed as 1 kHz. The dashed line illustrates the theoretical curve of Rayleigh-Lamb (RL) dispersion relation. (b) Observed resonant drop diameter (■) as a function of applied frequency. The mode number is fixed at 4. The solid line is a linear regression of data. The inset image shows polyhedra with mode number, $n = 4$, under different applied frequencies: from left to right, $f = 5$, 4, 3, 2, 1.5, and 1 kHz, respectively.

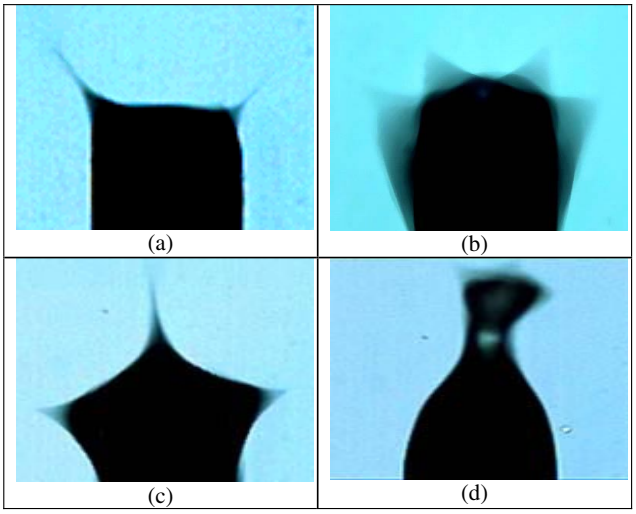

FIG. 4 (color online). Comparison between dc and resonant and nonresonant ac electrosprays. The separation distance between the needle and ground electrode is 10 mm. (a) Typical dc ramified mode at 3 kV. (b),(c) Resonant ac electrosprays at $f =$ 1 kHz, 3 kHz, $V_{\mathrm{rms}} = 900$ V. (d) Typical ac electrospray without a well-defined Taylor cone at 1.2 $\mathrm{kV_{rms}}$, $f = 8$ kHz.

mode numbers, the drop dimension is not much larger than the needle diameter and the drop is severely constrained. This accounts for the 5% discrepancy between the experimental result and the RL prediction in that range. The larger discrepancies at high mode numbers, 5 and 6, are probably because of gravitational effects of the larger drop dimensions, which are not included in either the RL formulation or the constrained drop model. Figure 3(b) plots the drop radius of the same mode number taken from six independent sets of experiments as a function of the applied frequency f. For fixed mode number n, the droplet diameters is proportional to $f^{-2/3}$, with a theoretical slope of 14 (SI units) for acetonitrile from the RL relation. Collapsing the measured data, which exhibits the correct frequency dependence, gives rise to a regressive slope of 13.7.

At higher voltages, the polyhedra become unstable and transient Taylor cones with liquid ejection appear at the polyhedral vertices in each half cycle. These transient Taylor cones begin to interact at even higher voltages shown in Fig. 4 such that they flicker violently. Figure 4 compares images between ramified drop fission modes of dc sprays (a) and resonant ac sprays with transient Taylor cones (b),(c) and nonresonant electrospray (d) without well-defined cones. Unlike its dc counterpart, the cones of resonant ac sprays are not confined to the orifice edges where the electric field is the strongest, but are evenly distributed over the entire meniscus, at roughly the antinodes or the vertices of the transient polyhedra [15]. Even though there are multiple transient Taylor cones for resonant ac sprays, the individual cone volume of each cone [Figs. 4(b) and 4(c)] can be larger than the dc cone [Fig. 4(a)]. Moreover, the onset voltage of multicone spray with ac resonance is found to be lower than its dc equivalent. However, it is also seen that the resonance and transient Taylor cones are favored more at low frequencies and are not observed beyond 10 kHz. As shown in Fig. 4(d), when the frequency is increased to 8 kHz, the Taylor cones are replaced by a smooth drop and a single liquid jet is ejected at the tip of the drop as in high-frequency ac electrosprays studied earlier [6]. This might suggest the presence of a resonant frequency for optimum ac electrospray throughput corresponding to the coincidence of f_{DL} with the drop resonant frequency f_1. In addition, the flow rate of resonant sprays shown as Fig. 4(b) is measured to be 3 μL/ min approximately, which can be an order of magnitude higher than the dc counterpart under similar conditions. However, further quantification is needed in order to understand the spraying behavior at this frequency range and the effect of resonance on it.

[1] J. B. Fenn, M. Mann, C. K. Meng, S. F. Wong, and C. M. Whitehouse, Science **246**, 64 (1989).
[2] G. Loscetales, A. Barrero, I. Guerrero, R. Cortijo, M. Marquez, and A. M. Ganan-Calvo, Science **295**, 1695 (2002).
[3] O. V. Salata, Curr. Nanosci. **1**, 25 (2005).
[4] S. B. Sample and R. Bollini, J. Colloid Interface Sci. **41**, 185 (1972); J. P. Borra, Y. Tombette, and P. Ehouarn, J. Aerosol Sci. **30**, 913 (1999).
[5] A. M. Gañán-Galvo, Phys. Rev. Lett. **79**, 217 (1997); M. Gamero-Castaño, Phys. Rev. Lett. **89**, 147602 (2002).
[6] L. Y. Yeo, D. Lastochkin, S.-C. Wang, and H.-C. Chang, Phys. Rev. Lett. **92**, 133902 (2004).
[7] G. I. Taylor, Proc. R. Soc. London **280**, 383 (1964).
[8] D. Lastochkin and H.-C. Chang, J. Appl. Phys. **97**, 123309 (2005).
[9] A. Ramos, H. Morgan, N. G. Green, and A. Castellanos, J. Phys. D **31**, 2338 (1998).
[10] H. Lamb, *Hydrodynamics* (Cambridge University Press, Cambridge, 1932), 6th ed.
[11] M. Z. Bazant and T. M. Squires, Phys. Rev. Lett. **92**, 066101 (2004); M. Z. Bazant, K. Thornton, and A. Ajdari, Phys. Rev. E **70**, 021506 (2004); T. M. Squires and M. Z. Bazant, J. Fluid Mech. **509**, 217 (2004).
[12] R. G. Holt and E. H. Trinh, Phys. Rev. Lett. **77**, 1274 (1996); R. E. Apfel, Y. Tian, J. Jankovsky, T. Shi, X. Chen, R. G. Holt, E. Trinh, A. Croonquist, K. C. Thornton, A. Sacco, Jr., C. Coleman, F. W. Lesile, and D. H. Matthiesen, Phys. Rev. Lett. **78**, 1912 (1997).
[13] A. J. James, B. Vukasinovic, M. K. Smith, and A. Glezer, J. Fluid Mech. **476**, 1 (2003).
[14] M. Strani and F. Sabetta, J. Fluid Mech. **141**, 233 (1984); **189**, 397 (1988).
[15] See EPAPS Document No. E-PRLTAO-97-044627 for resonant electrospray shown in Fig. 4(b). For more information on EPAPS, see http://www.aip.org/pubservs/epaps.html.